# INVESTIGATING CRACK PROPAGATION OF PEDOT:PSS IN AN ORGANIC/INORGANIC HYBRID SOLAR DEVICE

By

Kyle C. Abrahamson

* * * * * * * * *

Submitted in partial fulfillment
of the requirements for
Honors in the Department of Mechanical Engineering

UNION COLLEGE

June, 2011

*Forward*

The Department of Mechanical Engineering at Union College in conjunction with the Department of Chemistry and Biological Sciences are presently involved in the research and development of thin film solar nanocomposites. The thin film solar nanocomposite solar devices offer a cheaper alternative to solar technology, however the efficiencies of these thin film solar devices are very low compared to their silicon-based counterparts. The group's ultimate goal is to produce a flexible solar cell with efficiencies that are comparable to traditional silicon-based solar cells.

The collaboration of the Department of Mechanical Engineering at Union College has provided new insights that could help increase the development of solar nanocomposites. While there has been significant research on fabrication techniques, this project proposes to investigate the mechanical properties of the solar cell design, specifically the PEDOT:PSS/PET:ITO interface, to determine a correlation between interfacial interactions and overall efficiency. The report answers the following questions:

1. Does the mechanical strength of the PEDOT:PSS affect the overall efficiency of the device?

2. Will interfacial interactions and deformation between PEDOT:PSS and PET:ITO affect the overall strength of the device?

The purpose of this report is to state the conclusions obtained in my investigation. The Department of Mechanical Engineering is interested in how the cathode acting layer, PEDOT:PSS, and the PET:ITO interface influence photophysical properties and mechanical reinforcement. The knowledge gained from these further studies will also be of considerable interest in the design and fabrication of solar nanocomposites.

*Executive Summary*

The goal of this project was to investigate the mechanical strength and crack propagation of PEDOT:PSS under tensile loading, developing a correlation between these properties and the efficiency of the device.

*Results of Investigation*

Through the use of the tensile stage, a technique was developed to characterize the PEDOT:PSS material within the solar device. As PEDOT:PSS's mechanical properties are unknown, it was necessary to refine the technique with a material with known mechanical properties. Steel was used for the initial testing in order to develop the method necessary for accurate results. After tensile testing steel, the PEDOT:PSS/PET:ITO specimens were tensile tested and characterized. The PEDOT:PSS/PET:ITO specimens had Young's Moduli of around 422 ksi, which is in the accepted range of PET. The SEM characterization revealed crack propagation of the PEDOT:PSS layer after tensile testing.

*Conclusions and Recommendations*

1. Methods for material characterization and fabrication of each specimen were determined for quality control.

2. Young's Modulus was determined for steel and PEDOT:PSS/PET:ITO by the tensile stage and photogrammetry set up.

3. A full SEM characterization of untested and tested PEDOT:PSS/PET:ITO specimens was completed.

On the basis of these findings, a complete SEM characterization of PEDOT:PSS/PET:ITO specimens undergoing tensile testing is recommended. Tensile testing PEDOT:PSS/PET:ITO specimens under the SEM would allow for the user to mechanically characterize when crack propagation begins. This knowledge will help determine at what loads the PEDOT:PSS layer begins to fail and the different applications the solar cell can withstand without affecting its efficiency. After investigating PEDOT:PSS, a complete characterization needs to be performed on all the nanocomposite layers of the solar cell. The mechanical properties of each solar material will impact the overall solar device properties, which could affect the overall efficiency of the solar device. Once the solar device has been fully characterized, fabrication techniques of the solar device can be observed with respect to their mechanical properties and layer to layer interactions.

# TABLE OF CONTENTS

# TABLE OF FIGURES

# TABLE OF TABLES

# 1. Introduction

Throughout the world's history, humans have made leaps and bounds in energy technology. However, unfortunately there have been little improvements in alternative energy technology in the last few decades. Currently around the world, fossil fuels make up around eighty percent of the energy consumed annually [23]. Petroleum makes up approximately thirty-five percent of the fuel consumed annually. Experts predict that Petroleum will begin to peak in production in this decade, and this peaking will lead to significant gas price hikes and oil decline and depletion in approximately thirty to forty years [23]. The near-future depletion of fossil fuels and our strong dependence on them have raised many concerns about future alternative energy sources. Solar energy research has become a front-runner in alternative energy due to its high potential. For example, there's more energy from sunlight striking the earth in one hour ($4.3 \times 10^{20}$ J) than all the energy consumed on the planet in a year ($4.1 \times 10^{20}$J) [1]. In the remainder of this Introduction, a brief history of energy advancement will be presented.

## *1.1 Past, Present, and Future Trends of Energy Consumption*

At the beginning of humanity, the main source of energy was fire. In ancient Greek mythology, it was believed that Prometheus, a titan immortal, stole fire from Zeus in order for humans to use, and this single act started the innovation of harnessing energy. Actually, archeologists believe fire was first harnessed over two-hundred and fifty thousand years ago while true humans, homo sapiens, appeared only one-hundred and sixty thousand years ago [2]. So, the discovery of fire precedes the first existence of modern humans; however, once modern humans had fire in their hands they engineered ways to improve this fuel.

Wood was the main fuel for fire for hundreds of thousands of years. In order to harness the energy of fire, wood was the only fuel source for early humans. The abundance of forests all

over the world, especially around Europe, allowed early civilizations easy access to fire [2]. Wood continued as a major fuel source for humans from early civilizations, like the ancient Greeks, all the way to the Middle Ages. However, the scarcity of wood and high demand for energy would lead humans to find other sources of fuel, like coal.

Coal was another early fuel source discovered by human, and this fuel will become a major energy source for the world still used today. Coal was first used by ancient Romans as fuel for funeral pyres [2]. The Romans had access to all the major coalfields around England and Wales for hundreds of years, and Englishmen would continue to harness the fuel after the fall of the Roman Empire [2]. Coal was also used in iron-working and many other forging processes through the Roman Empire all the way to the Middle Ages [2]. However, wood was more available than coal, and that's the reason coal was never a major fuel source until the 16$^{th}$ century. In the 16$^{th}$ century, the English Parliament passed a Preservation of Woods Act in order to preserve lumber due to the huge expansion of population growth, agricultural productivity, and colonial exploration [2]. Coal became a cheaper, more abundant, and easy accessible alternative to wood as an energy source [2]. Coal would eventually become the main source of energy in England throughout the seventeenth century, and reached its peak during the Industrial Revolution in the nineteenth century. This transition of energy fuel created new innovations, such as the steam powered engine, that were necessary for the new power source. This spark of innovation and engineering wouldn't stop with coal, but continue on when petroleum hit the scene.

The transition from coal to petroleum would bring many new innovations that humans use today. Once the Industrial Revolution was in full swing, factories and businesses had a huge demand for "artificial lighting" [2]. Since whale oil has become scarce and kerosene (from coal)

was expensive at the time, entrepreneurs and geologists, like Benjamin Silliman Jr., started to analyze crude oil and see the possible products it could produce [2]. Silliman concluded that crude oil could produce "very valuable products," such as lamp oil and lubricants, and so the boom of oil drilling started soon afterwards during the mid-nineteenth century [2]. This new source of energy helped create new innovations, like the internal combustion engine (ICE) and Petroleum would ultimately take over as the main source of energy during the twentieth century. The problem with these energy sources like coal and Petroleum is that they are not renewable.

In the twenty-first century, the push for alternative energy advancements has become important because of the near-future depletion of fossil fuels [6]. Just to overview past and present energy consumption trends, the U.S. and most of the world has transitioned from wood to coal to petroleum as major primary energy sources over the years. There have been a few other sources of energy added over the last century, such as natural gas, nuclear, and hydroelectric (Figure 1).

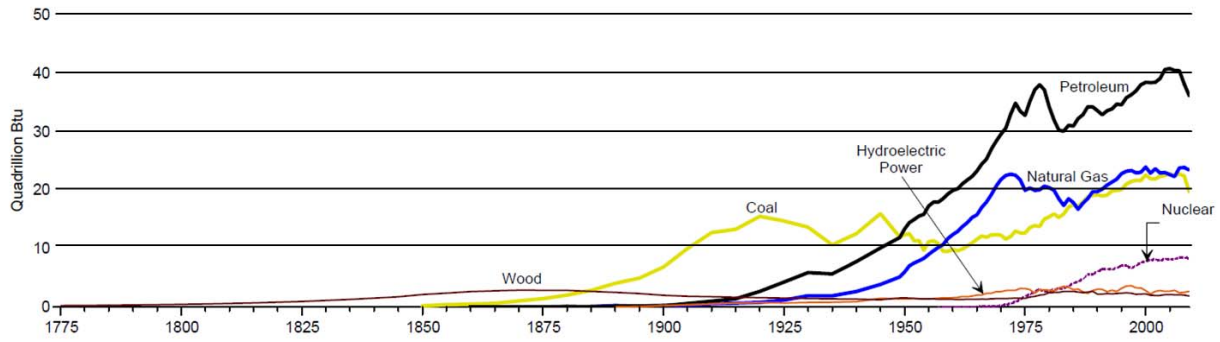


**Figure 1: U.S. Primary Consumption by Source, 1775-2008, EIA Annual Review 2009 [4].**

Besides seeing the demand for energy increase heavily over the last thirty years, our supply of major energy sources are running out. The U.S. primary consumption plot shows Petroleum, natural gas, and coal all reaching a peak. This peak of maximum production is known as Hubbert's peak [23]. Hubbert's peak theory predicts that after peaking the rate of production

of a fossil fuel would then enter a terminal decline [23]. Many experts have been predicting the peaking of major fossil fuels, like coal and Petroleum, have already started around the globe [3]. The decline of major energy sources has started the search for abundant, renewable energy sources.

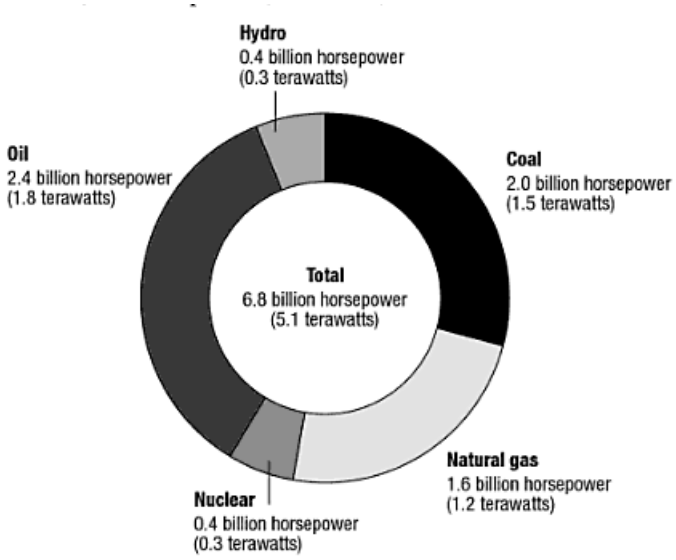


**Figure 2: World Power Consumption, by Primary Energy Source, BP Statistical Review of World Energy 2009 [4].**

Currently, fossil fuels such as oil, gas, and coal constitute over 80% of the world's marketed demand for energy services today [2]. According BP Statistical Review of World Energy 2009, oil, gas, and coal make up 88% of the world's energy sources for consumption (Figure 2). In 2008, the world consumption of oil was around 85 million barrels daily, while the world oil reserves were approximated at 1,243.6 billion barrels (1,623.6 billion barrels with oil sands) [2]. If the world consumption rate stays at this rate, then it would take only approximately 42 years (55 years with oil sands) to go through the remaining world oil reserves. The world's oil consumption rate is increasing due to emerging economies like China and India that are growing at unprecedented rates. The growing needs of energy for emerging economies, like China and

India, will only mean more dependence on finite energy sources, like coal (Figure 3 and Table 1).

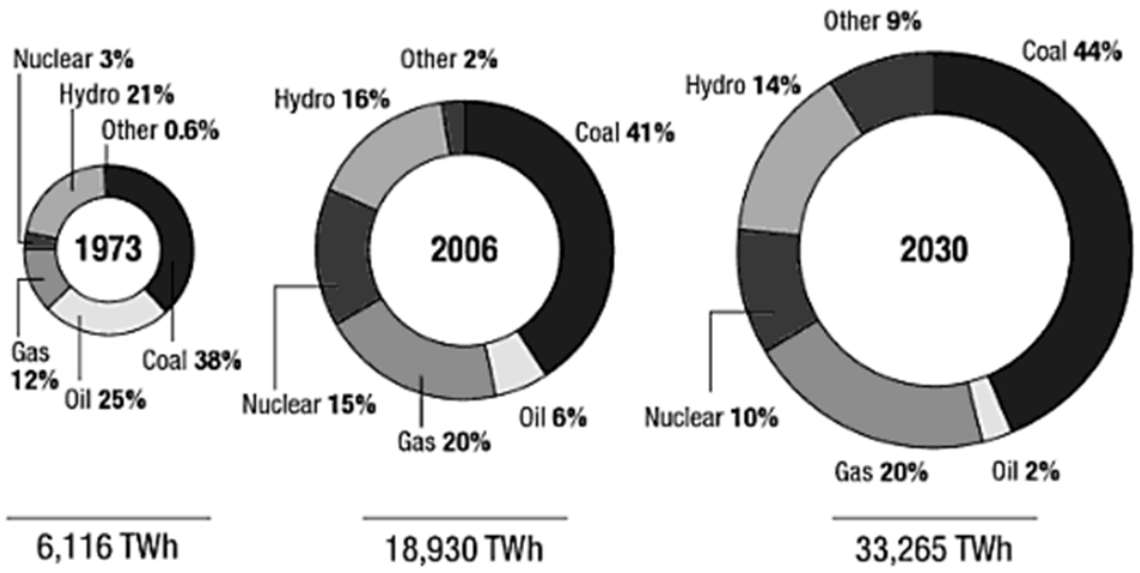


**Figure 3: Global Electricity Generation, by fuel, 1973, 2006, and Projected 2030, IEA World Energy Statistics 2008 [4].**

**Table 1: Top Five Countries with Largest Coal Reserves, BP Statistical Review of World Energy 2009 [4].**

| *Country* | *Reserves (million tons)* | *Percentage of world total* | *Reserves-to-production ratio** |
|---|---|---|---|
| US | 238,308 | 28.9% | 224 |
| Russia | 157,010 | 19.0% | 481 |
| China | 114,500 | 13.9% | 41 |
| Australia | 76,200 | 9.2% | 190 |
| India | 58,600 | 7.1% | 114 |

According to the International Energy Agency Key World Statistics 2008, electricity consumption has increased by 210% from 1973 to 2006 [4]. From 2006 to 2030, world electricity consumption is predicted to increase 76% [4]. However, coal is predicted to make up 44% of the fuel used to generate electricity in 2030, which is 3% higher than in 2006. The problem with present and future electricity consumption trends is the global reliance on finite energy sources that will be deleted in the near future and also cause environmental pollution.

From these predictions, other fuels for global electricity generation will increase 7% from 2006 to 2030, but it's crucial now to produce some alternative sources of energy.

*1.2 Alternative Renewable Energy Sources*

Over the past decade, there have been major contributions made in researching the possible alternative energy solutions of the future. Between 2002 and 2008, private global investment in renewable energy went from a trickle to a torrent, from a few billion dollars to over $100 billion and 2.4 million jobs [2]. Also, nearly all advanced nations, and many states in the U.S., now have policies mandating renewable energy for 10% or more of power generation [3]. Even though these advancements were made based on ways to offset effects of carbon dioxide from fossil fuels towards global warming, which is debatable, the more important issue is the need for alternate sources of energy due to the scarcity of fossil fuels. Just like in the 16$^{th}$ century England, there have been policies and taxes that have made fossil fuels more expensive and scarce. In this uncertain transition period, many different alternative energy technologies have made major improvements, specifically in electricity and transportation.

Wind technology brings a fresh breath of air to the new possibilities of alternative renewable energy. The main component in wind technology is the wind turbine. Just to recap, a wind turbine is a rotary device that converts wind energy into mechanical and then into electrical energy. As one of the fastest growing industries in the decade, the wind industry has grown about 25%-30% a year from 2000 to 2008 [2]. For instance in wind technology, a new wind turbine design from FloDesign Wind Turbine Inc. has been designed and analyzed to utilize all possible energy from the wind using a nozzle-ejector design while supposedly breaking the Betz' limit [5]. There may be a shift in the air for alternative energy; however, there are some drawbacks with wind. Unlike water currents, wind patterns are very hard to predict just like have a

meteorologist trying to predict the weather in New England, and the storage of unused energy has also been a big concern. In this uncertainty, investors may decide to go with bio-fuels and place bio-crops where the wind farms could go.

Bio-fuels have become the most promising and reevaluated alternative energy source in recent memory. Bio-fuels, like ethanol and biodiesel, became huge alternative fuels of interest during 2003 [3]. The main reason for bio-fuel research was to help offset the harmful effects of petroleum to the atmosphere, which isn't as important as the advantages these new bio-fuels bring to energy advancement. Besides being "supposedly" less polluting than petroleum, these bio-fuels allow for the world to keep their transportation sector intact, so no overhaul of a new engine in cars. However, bio-fuels, like ethanol and bio-diesel, are less efficient than gasoline. For instance, it takes 1.5 gallons of ethanol to get the same work as one gallon of gas [2]. Ultimately, bio-fuels don't offer an energy improvement over oil, which makes them hard to bring to market. Also, it is projected that only about 5% of the land on Earth would be realistically possible for bio-energy crops [2]. Unfortunately, studies have shown that the habitat change due deforestation created by this bio-fuel craze in order to plant bio-crops has made bio-fuels more polluting than petroleum [2]. After these comments about bio-fuel, maybe it's time humans started looking elsewhere, like below the surface of the earth.

Just like "global warming," energy possibilities about geothermal energy are starting to heat up. Just to summarize, geothermal energy is the process of extracting heat in the Earth's interior. Geothermal energy has been used for centuries, including in ancient Roman times when Pompeians used geothermal energy, a.k.a. Mount Vesuvius, to heat their homes [2]. Just like in wind technology, the purpose of extracting this internal heat is to then turn a fluid, like water, turn it into a vapor to drive a turbine to turn the heat into mechanical energy then into electrical

energy. The advantage of geothermal energy besides being free like wind and solar, but it's more constant source of energy [3]. The drilling technology for geothermal energy would be the same as oil/gas drilling, and any country with recent volcanic and igneous activity have resources to this energy [2]. However, there is also a drawback, minor though. The renewable energy community compares geothermal energy similar to oil/gas extraction, and the drilling and fracturing of the earth is frowned upon as inferior to other alternatives such as wind and solar [2]. Even though drilling can be complicated and one mistake could be catastrophic, but it would be interesting to see what the future brings to geothermal energy due to its long history and promising potential. However, the potential power of the geothermal heat doesn't compare with the potential power from the sun.

### *1.3 Solar Energy Advancement*

Solar energy has become one of the biggest alternative energy sources being researched today. Technically, all of the energy, including nuclear and geothermal, all originates from the sun [2]. However, that statement may be true, but the end result is there are different types of energy sources throughout the world. In terms of solar energy, there're three basic ways to extract solar energy used today: solar thermal systems, "passive solar," and photovoltaics. A solar thermal system involves lenses or mirrors to intensify solar radiation, heat a fluid, and generate electricity [2]. For example, one could concentrate enough heat to create steam and drive a turbine generator to produce electricity. A "passive solar" system allows for sunlight to naturally illuminate and warm the insides of structures, like sun-facing windows and walls [2]. Lastly and widely known, a photovoltaic (PV) solar design uses semi-conductor material, usually in cells, to produce electricity [6]. Let's look at the photovoltaic solar design.

Photovoltaic solar cells have made their mark as an energy source throughout the world in the past and present. In 1873, British scientist Willoughby Smith studied the photo-sensitive properties of selenium, and he concluded that selenium's ability to conduct electricity increased in direct proportion to the degree of its exposure to light [6]. Later in 1905, Albert Einstein offered his explanation of the photoelectric effect, which in turn led to the development of the photovoltaic effect [6]. The photovoltaic effect involves generating electrons that are then transferred from the valence bands to conduction bands within a material (like silicon), which results in the buildup of a voltage between two electrodes in the cell. In 1954, Bell laboratories invented the first silicon-based PV solar cell, while later in the 1950's NASA installed a PV system on the United States' first satellite, Vanguard I [6]. Today, PV solar technology is used to power residential homes, spacecrafts, satellites, utility power, and many other applications. Let's review on how the photovoltaic cells convert sunlight into electricity.

Just to recap, photovoltaic (PV) cells utilize the photovoltaic effect, explained above, to convert sunlight into electricity. In a more specific case, there are p-n junction solar cells that after sunlight exposure produce an electric current due to the excited electrons and remaining holes, cations, are swept in different directions by the built-in electric field of the depletion region [6]. Just to clarify, p-type semiconductors have an abundance of holes or protons like in a silicon lattice, while an n-type semiconductors have an abundance of electrons or negatively charged carriers. In silicon p-n junction solar cells once the photons excite electrons in the solar cell, this causes a drift of electrons from the negative n-type side of the cell into the positive p-type side of the cell and the holes drift in the opposite direction, which in turn creates a voltage across the cell [6].

**Figure 4: Example of Silicon-Based Photovoltaic Cell, Source: solarnavigator.net.**

Currently in solar technology, silicon-based photovoltaic solar cells make up 95 percent of solar technology market (Figure 4). The silicon-based solar cells in today's market have moderate efficiency, ranging from 12%-25%. However, these current solar cells are expensive compared to other fuels used to produce electricity. These high costs are due to the material costs of silicon and also the complex fabrication process (Figure 5).

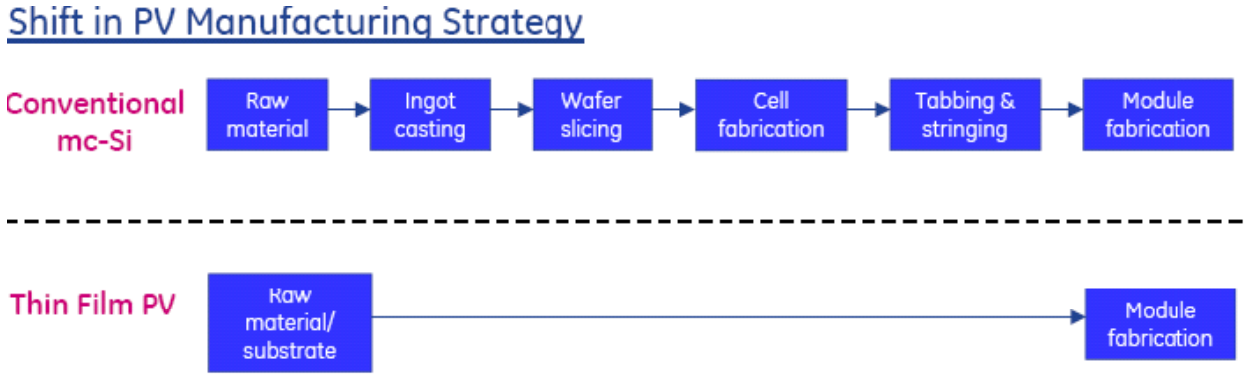


**Figure 5: The manufacturing process of conventional silicon based solar cells and thin film materials [8].**

Current silicon-based photovoltaic cell technology cost around $0.3/kW while other fuels used to produce electricity, like coal and nuclear, only cost around $0.05/kW [4]. So, solar technology is currently six times more expensive to produce than current electricity sources. These extremely costly silicon-based photovoltaic cells have moderately low efficiency rates [2].

The recent development of cheaper alternatives to silicon, such as nanocomposite materials, in PV solar cells has become a hot topic of discussion.

*1.4 Flexible Solar Nanocomposite Photovoltaics*

Although silicon solar cells are the most common type of photovoltaics, thin-filmed, solar nanocomposite devices are beginning to receive a considerable amount of funding and attention. A thin-filmed solar cell is defined as a solar cell that is made by depositing one or more thin layers (thin film) of photovoltaic material on a substrate (Figure 6) [1]. Solar cells have diverged into several different categories including dye-sensitized solar cells, polymer-based solar cells, nanocrystal solar cells and hybrid solar cells [9]. Currently, the most common thin film materials includes amorphous silicon, cadmium telluride and copper-indium-gallium diselinide [1]. Thin films differ from the conventional silicon-based solar cells because they have different materials for both the *p* and *n* junction layers; furthermore, they can have up to three semiconducting layers that can create higher output voltages.

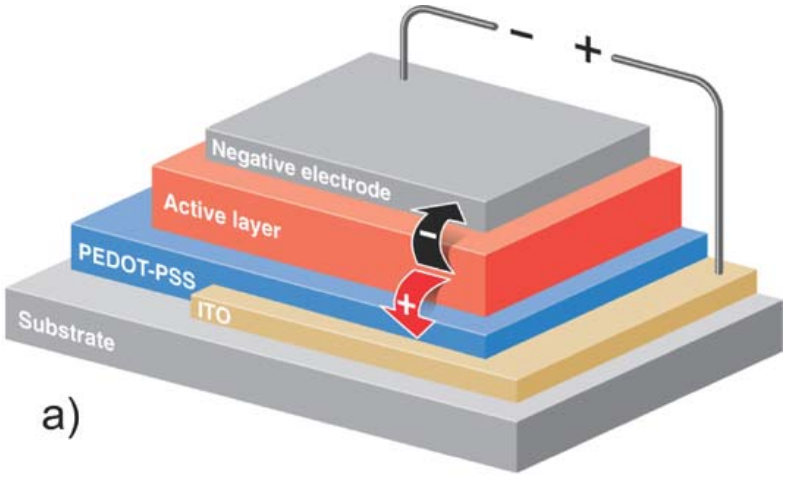


**Figure 6: Example of Thin-Filmed Solar Cell, Source: http://spie.org/x14269.xml?ArticleID=x14269.**

Flexible, solar nanocomposite photovoltaic solar cells have the potential being as or more efficient than their silicon-based photovoltaic (PV) counterparts while being a cheaper

alternative. The one big problem with flexible, thin-filmed nanocomposite solar cells is the low efficiency rates, ranging from 5%-12% [2]. Even though cheaper materials and manufacturing techniques are used in these thin-film, nanocomposite photovoltaic cells, the efficiencies of these cells are too low to even consider bringing them to the economic market.

The Department of Chemistry and Biological Sciences is currently developing and researching a hybrid organic-inorganic bulk heterojunction and bilayer thin film solar cell involving quantum dot based electron-hole separation. These quantum dot based solar cells offer remarkable photo efficiencies, tunable surfaces to optimize charge transfer, multiple exciton generation, and broadband absorption of the solar spectrum [7]. This nanocomposite solar cell consists of multiple layers with p-type semiconductor, n-type semiconductor, and light-absorbing properties to produce a voltage across the solar cell. These new solar cells would be excellent for new applications, however there's very little knowledge about these materials' mechanical properties.

### *1.5 Mechanical Characterization*

In order to investigate the layer to layer interactions of a solar device, specific mechanical testing must be done in order to understand how these layers will perform under certain mechanical applications. Tensile tests have been completed in the molecular range of certain nanocomposite materials and have resulted in accurate calculations for Young's modulus. The mechanical properties obtained by these tests have accurately proven that Newtonian mechanics can describe the underlying physics at the nanoscale for polymeric based nanocomposites [10]. While the mechanical properties of some of the polymeric material encapsulated in the solar cell have been determined, they have not been closely examined with regards to solar applications.

The mechanical properties of these flexible, solar nanocomposite solar cells could help understand the limits of certain stresses and loads that might occur on these thin-filmed solar cells under different applications. The most important aspects of these nanocomposite solar cells are the interfaces between the different layers. If under certain conditions (like tension or compression) in nature, the interfaces between each of the layers might alter due to deformation or crack propagation, which in turn could ultimately mean lower efficiency or failure of these solar cells. The Department of Mechanical Engineering at Union College is doing extensive research to understand the mechanical properties of these solar cell's layers and to make connections with these properties with solar cell efficiency and improving the solar cell.

# 2. Literature Review

While our dependence of energy has become a growing concern with the future depletion of fossil fuels, solar technology brings an abundant and renewable energy source for future generations. However, solar technology has big issues to solve before becoming a prominent energy source for the world. The high cost of silicon-based photovoltaic solar cells due to production costs, material costs, and moderately low efficiencies have made solar technology a tough sell in the financial market. These thin-filmed photovoltaic cells have huge promise, but thin-film cells present research challenges in designing materials and in understanding the electronic and molecular basis of capture, conversion, and storage before its promise can be realized [11]. In this chapter, the PEDOT:PSS layer of the nanocomposite solar cell will be thoroughly investigated with respect to the mechanical properties and electrical properties and how improvements have been made to increase the hole-conducting properties of this layer in the solar cell. Furthermore, as the goal of the project is to investigate the mechanical properties of the solar nanocomposite layer PEDOT:PSS, one characterization method is presented along with the group's results. Lastly, their results will be compared to experiments that will take place in this project.

## *2.1 Solar Cell Layer Characteristics*

The hybrid organic-inorganic bulk heterojunction and bilayer thin film solar cell developed at Union College is composed of multiple nanocomposite layers. The solar cell will have a plastic substrate, rather than the conventional glass substrate. The materials present in the organic-inorganic bulk heterojunction developed at Union College allows for adequate absorption and emission behavior, stability against photo bleaching, flexible molecular coupling, multiple exciton generation and high quantum yields [7]. These materials have specific roles in

the photovoltaic process, and each material's characterization will be discussed later in this section. An illustration of all the materials present in the solar cell is shown in Figure 7.

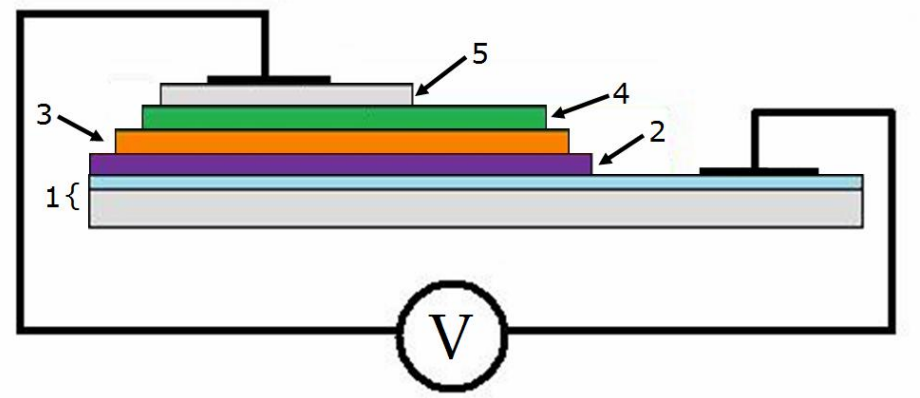


**Figure 7: An illustration of the Hagerman solar cell. 1-ITO coated polyethylene substrate, 2-PEDOT:PSS, 3-Laponite/CdSe, 4-Polyaniline, 5- Sputtered Aluminum alloy to complete the circuit [9].**

This hybrid solar cell is assembled layer-by-layer onto a plastic substrate, a flexible polyethylene terephthalate (PET) based substrate. PET is a plastic polymer that is transparent and flexible, which will allow for flexible applications that glass-based solar cells could not withstand. The PET is covalently bonded with a transparent chemical compound known as indium tin oxide (ITO) through electro polymerization [12]. ITO's main feature is the combination of electrical conductivity and optical transparency, which is ideal for the photovoltaic effect. The PET and ITO are depicted as the gray layer and blue layer respectively in the composite layer number 1 in the above figure (Figure 7). Once this ITO layer has bonded to the PET substrate flex material, aluminum particles are sputtered onto the ITO to complete the necessary circuit in order to create a voltage throughout the cell.

On top of the PET:ITO substrate, Poly(3,4-diethylenedioxythiophene) (PEDOT) is the hole conducting polymer or *p*- type (positive) material that has electrical conductivity properties. The addition of poly (styrenesulfonate) (PSS) yields a soluble composite that forms thin films with the same conductivity properties [9, 12]. The combination of PEDOT rich shells and PSS

chains create a polymer that is highly stabile and conductive, which helps increase the efficiency of polymer photovoltaic devices. This layer helps the solar device through facilitating the hole injections which prevent electron movement into the ITO. Hole injections make the ITO the cathode, positive side, of the solar device. The PEDOT:PSS layer is shown as purple layer 2 in the above figure (Figure 7); furthermore, its chemical structure is shown below (Figure 8).

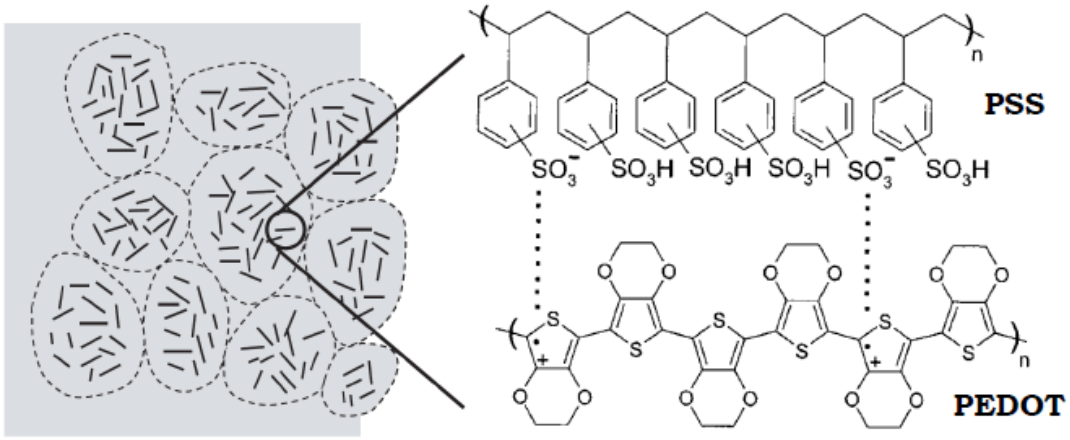


**Figure 8: Left: cartoon representing the top view of the morphology of a thin film of PEDOT:PSS particles, surrounded by a thin PSS-rich surface layer. PEDOT chains are displayed as short bars. Right: chemical structure of the species present in the film [21].**

The next layer, orange layer number 3, of the solar device is Laponite, which is a synthetic clay which creates an inorganic scaffold to host the active layer of the solar cell. Laponite nanoparticles consist of disc like shapes with a radius ranging from 25-40nm and a height of about 0.92nm [15]. It serves as the active host for electron charge transport, while the exciton formation occurs because of the CdSe [13]. Furthermore, Laponite has the ability to form a sol, a gel or a thin film and is capable of hosting guests such as quantum dots into its matrix [14]. Quantum dots are ideal for LED and solar cell applications owing to their tunable absorption and emission behavior, stability against photo bleaching, flexible molecular coupling, multiple exciton generation and high quantum yields [7]. In photovoltaic applications, this layer

contributes the excited, valence electrons that will diffuse through the solar device and cause an electric current.

The next layer of the solar device is Polyaniline (PANI) material, which is a polymeric based material that has several characteristics needed to help produce a successful voltage difference throughout the entire cell. PANI is the electron conducting polymeric material, or the *n*-type (negative) material and is represented as the fourth green layer in the above figure (figure 7). PANI has attracted much attention as it offers high conductivity, environmental stability, simple manufacturability, coupled with versatility for design and fabrication of nanocomposites [7]. PANI provides an easier means of processing and forming conductive products as well as providing low cost solutions for the production of transparent thin films [7]. In order to complete the circuit through the device as mentioned before, a layer of aluminum is sputtered onto the PANI layer and attached to the ITO layer.

After analyzing the material characteristics of this solar cell, this project will undergo characterizing the PEDOT:PSS layer in this thin-filmed solar cell and its layer to layer interaction with ITO. Understanding the mechanical properties and characterization of PEDOT:PSS and ITO layer to layer interaction will help researchers understand how this interaction will respond to certain mechanical applications including certain fabrication processes. Finding ways to simplify the solar cell fabrication process is just as important as improving the overall efficiency of the solar device, since both would ultimately drive the cost of solar technology lower. The different fabrication techniques that could be used for this thin-filmed solar device will be discussed in the next section.

*2.2 Solar Cell Fabrication*

Polymer thin-filmed solar cells have appealed to researchers due to their flexibility, light-weight, and low-cost; however, polymeric semiconductor-based solar cells do not perform as efficiently as their organic counterparts [9]. One of the goals of this project is to investigate the morphology and characterization of the nanocomposite layers of the solar cell. This morphology research will have a significant role in the design of flexible photovoltaic materials. The majority of their research includes analyzing various self-assembly fabrication techniques of thin film solar materials. Self-assembly has been described as the autonomous organization of components into patterns or structures without human intervention [16]. The simplicity of self-assembled solar cells will help in cutting costs for photovoltaic cells and future solar technology. Most research done with flexible, solar nanocomposites has been spin-coated onto a substrate; however the spin-coating technique is more complicated than various other techniques like spray-coating or inkjet printing techniques.

In order to maintain a smooth, uniform layer, a spray-coating or inkjet printing technique would be a better solution for thin film application than spin coating. Inkjet printing is a highly flexible technology that is able to deposit small amounts of material in a required pattern preset through digital part modeling without the need of costly patterning masks and can be scaled up for larger print size or quantities [22]. Material wastage in inkjet printing is kept to a minimum at about 2% [22]. However, one problem that occurs with any sort of thin film application process is keeping the uniformity of the thin film material during drying process. Even though the initial fluid surface is flat, we cannot be sure that the surface of the dried film is also flat [22]. There have been studies done in order to analyze the effect of substrate temperature and drying process

of nanocomposite materials, like PEDOT:PSS. From these studies, the dried drop of PEDOT:PSS surface tends to become flat  in the experiment around 40°C to 45°C (Figure 9).

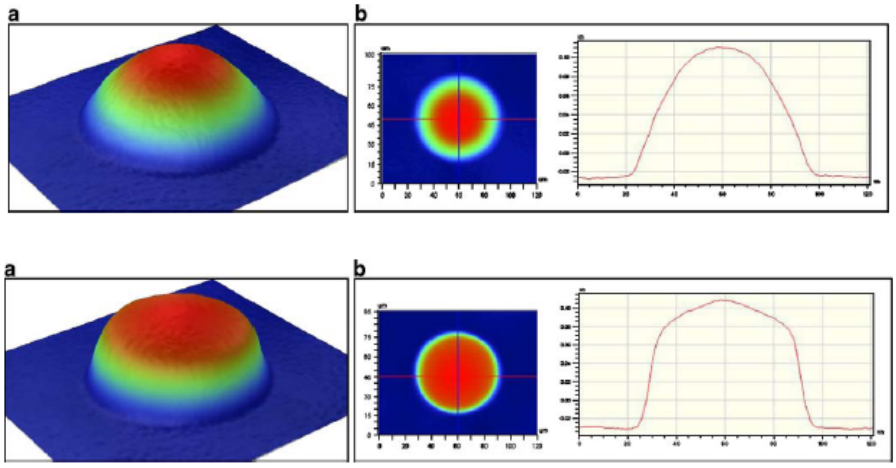


**Figure 9: Top: (a) 3D image at 40°C; (b) 2D cross-sectional profile and top-down view at 40°C, Bottom: a 3D image at 45°C; b 2D cross-sectional profile and top-down view at 45°C [22].**

However, any lower or higher substrate temperature would cause the PEDOT:PSS dried droplet to become a Gaussian shape of ring-like shape respectively [22]. A Gaussian profile is a dried droplet in the shape of a simple cap, not a flat top. A ring-like structure involves a distinct ring-like pattern starting to be formed with higher edges and lower centers. These two types of droplet profiles would cause a non-uniform PEDOT:PSS layer that would ultimately effect the layer to layer interaction with other nanocomposite layers and the efficiency of the solar device.

While the techniques of fabrication used to assemble these materials are currently under constant scrutiny, certain aspects such as the mechanical properties of each material have been ignored. Mechanical properties such as stress, strain and modulus have not been explored with regards to photovoltaic applications; the properties of each material could impact the architecture of the cell as well as the method of assembly. Tensile test is a methods used for mechanical characterization. Tensile testing on casted PEDOT:PSS is described in detail in the following section.

*2.3 PEDOT:PSS Tensile Testing*

There was a study done on the electrical conductivity, tensile properties, electromechanical response and moisture sorption isotherm of PEDOT:PSS casted films at the Interdisciplinary Graduate School of Medicine and Engineering at University of Yamanashi. Many researchers used two specific ways to investigate the mechanical properties of thin-film structures, either tensile testing of multilayered compounds or tensile testing of single layer specimen. Thin film structure research across the world has generally focused on multilayered structures [17]. A few advantages of this test includes stress state relevant to flexible electronics, ease of fabrication, no third-body interaction and measurement of adhesion possible [18]. In contrast, some disadvantages of this test are indirect information on the failure mode as well as a difficult determination of Young's modulus and tensile strength of materials of the multilayer [18]. Also, as multi-layers are investigated, complicated mechanical stresses occur at the interfaces that yield inaccurate results [18]. Tensile tests of single layer specimens are advantageous due to their uniaxial stress state as well as their direct measurements of Young's modulus and fracture strength of a single test specimen [18]. An overview of the mechanical testing methods for thin film structures can be seen in Table 2.

**Table 2: Overview of Mechanical Testing Methods for Thin Film Structures [18].**

| Test | Advantages | Disadvantages |
|---|---|---|
| Tensile test of multilayered compounds | • Stress state relevant to flexible electronics<br>• Ease of fabrication<br>• No third-body interaction<br>• Measurement of adhesion possible | • Indirect information on the failure mode<br>• Difficult determination of Young's modulus and tensile strength of materials of the multilayer |
| Tensile test of single layer specimen | • Uniaxial stress state<br>• Direct measurement of Young's modulus and fracture strength possible<br>• Size effects such as different thickness can be examined | • Difficult fabrication of single layer specimen<br>• Time consuming experiments |

A tensile test of single layered specimens was determined to be the most advantageous method to characterize the mechanical properties of thin polymer films under various environmental conditions. In the study at the University of Yamanashi, a tensile test of a single layer specimen, PEDOT:PSS, was chosen in order to precisely analyze the mechanical and electrical properties of this nanocomposite material. For the mechanical properties of PEDOT:PSS, this study investigated the Young's modulus, tensile strength, and elongation at break. Young's modulus is the ratio of linear stress to linear strain [19]. The experimental stress and strain gathered from each tensile test will be used to develop a micromechanical model. These devices will be subject to deterioration due to the environmental and human contact that could ultimately affect the efficiency of the solar device. For this reason, it's very important to understand the mechanical properties of each layer of the solar device.

For material fabrication, the PEDOT:PSS specimens were casted in a dish and allowed to solidify by evaporation of solvent and annealed at 160° C for one hour in a vacuum [20]. For testing, these PEDOT:PSS specimens were tensile tested in a tensile tester, EZ-Test Shimadzu, at a strain rate of 10%/min [20]. The importance of this tensile test was to analyze where PEDOT:PSS was going to fail under certain stress applications [20]. Also, the electromechanical properties of PEDOT:PSS specimens were measured with an electromechanical cell equipped with an inductive displacement sensor and temperature sensors [20]. The purpose of measuring the mechanical properties of PEDOT:PSS under electrical application to analyze the mechanical behavior of PEDOT:PSS and how this may affect how the material performs.

For mechanical results, the study found that PEDOT:PSS specimens had a Young's modulus, tensile strength, and elongation at break of 1.8 GPa, 57 MPa, and 10% respectively [20]. Unfortunately, the authors didn't include any stress-strain curves in their article for further

analysis. For electromechanical properties, the study concluded that PEDOT:PSS had a thickness and electrical conductivity of 21 μm and 3 S/cm respectively [20]. When a DC voltage of 20 V was applied to PEDOT:PSS, the film underwent significant contraction, strain of 0.9% or 0.5 mm, in response to the electric field [20]. But, when the electric field is turned off, the PEDOT:PSS film returns to its original length, which means the electromechanical properties of this material are reversible [20]. The strain (%), current (mA), and temperature of PEDOT:PSS undergoing the electric field test can be seen below in Figure 10 [20].

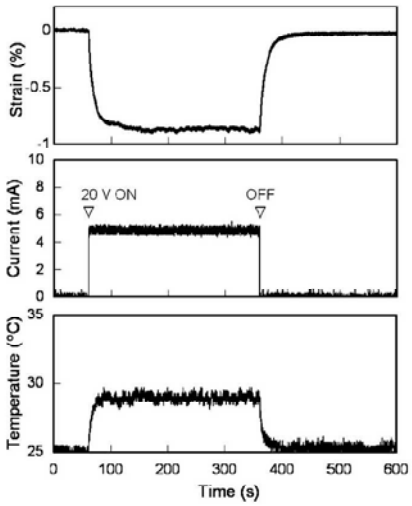


**Figure 10: Time profiles of strain, electric current, and surface temperature of PEDTO:PSS thin films under application of 20 V measured at 25° C and 50%RH [20].**

The study went on further to investigate the dependence of voltage on the strain, electric current, and temperature of the PEDOT:PSS films (Figure 11) [20]. The electric current exhibited a linear proportion to the applied voltage, so the PEDOT:PSS film is ohmic in the experimental range of the electric field [20]. However, temperature and more importantly strain increases with increasing applied voltage [20]. The PEDOT:PSS film reached a strain of 2%, which is twice as large as that of polypyrrole films [20].

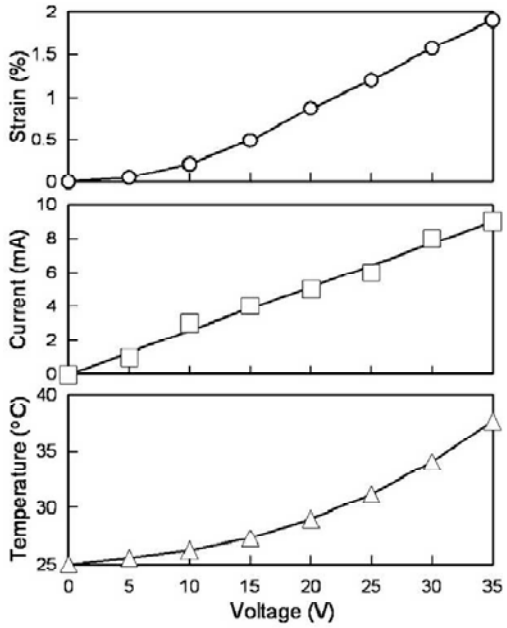


**Figure 11: Voltage dependence of strain, electric current, and surface temperature of PEDTO:PSS thin films measured at 25° C and 50%RH [20].**

PEDOT:PSS films undergo significant contraction when an electric field is applied [20]. More research must be done in order to analyze the mechanical properties of PEDOT:PSS to understand how it will degrade and fail under certain mechanical load applications. Furthermore, observing the mechanical behavior of the solar device can lead to a better understanding of layer interactions and the overall efficiency of the solar device. Characterization techniques such as photogrammetry and scanning electron microscopy of PEDOT:PSS were thoroughly examined. A tensile test was deemed to be the most effective method for mechanical testing and will be discussed in the following chapter.

# 3. Experimental Procedures

In this section, the experimental procedures to determine the mechanical properties of the PEDOT:PSS conductive layer in an multi-layer nanocomposite solar device will be discussed. Materials, like steel, ITO, and PEDOT:PSS, and various equipment, such as tensile stage, photogrammetry, and SEM, were needed in order to test and analyze the morphology and mechanical characterization. The mechanical characterization of PEDOT:PSS will determine the morphology, such as micro cracking, of PEDOT:PSS under certain stress applications, like tension or compression. This knowledge of PEDOT:PSS mechanical behavior under these different stresses will help understand how the solar cell will perform under different applications. Throughout this section, the various specimen fabrication techniques, tensile stage testing, photgrammetry analysis, and SEM analysis will be thoroughly explored.

## *3.1 Materials*

For this project, steel and PET:ITO/PEDOT:PSS specimens were fabricated using various cutting and application techniques. The steel sheets, ITO sheets, and PEDOT:PSS used for this project were acquired from previous senior projects. However, more PET:ITO sheets and PEDOT:PSS solution will be purchased from Solaronix and Sigma-Aldrich respectively. The ratio of PEDOT to PSS was approximately 1:2.5 respectively, and the PEDOT:PSS solution used was 1:5, meaning 1 part PEDOT:PSS to 5 parts of solution (4 parts water). The PET:ITO layers had a film thickness of 175 microns. For tensile stage testing and SEM/photogrammetry measurements, steel and PET:ITO samples were cut into precise “dog-bone” test specimens.

*Steel Specimen Fabrication*

The steel layers were cut into a specific geometric "dog bone" shaped specimens in order to correctly tensile test the steel specimens. This "dog bone" shape is favorable for mechanical stress and strain testing because it ensures that the failure in each material will occur in the center, where the maximum stress and strain will occur. The "dog bone" shaped specimen was designed with specific dimensions (Figure 12).

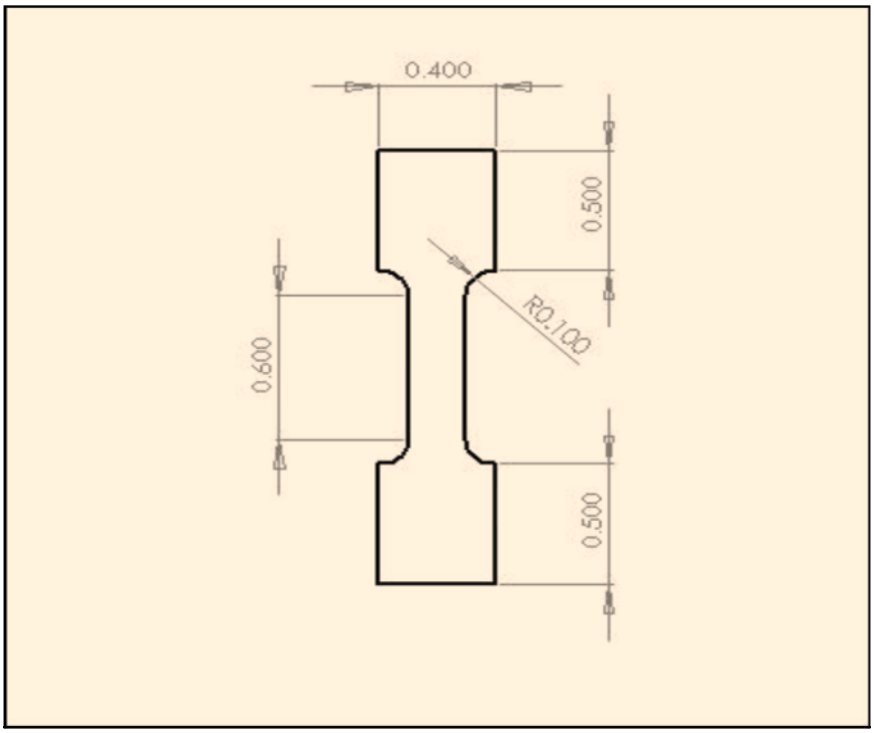


**Figure 12: Solidworks depiction of "dog bone" specimen with dimensions in inches.**

Using the specimen cutting platform designed by Todd Herman and James Howard of the Union College machine shop (Figure 13), the steel were milled using a drill press in the Union College machine shop into precisely sized "dog bone" shaped specimens (Figure 14).

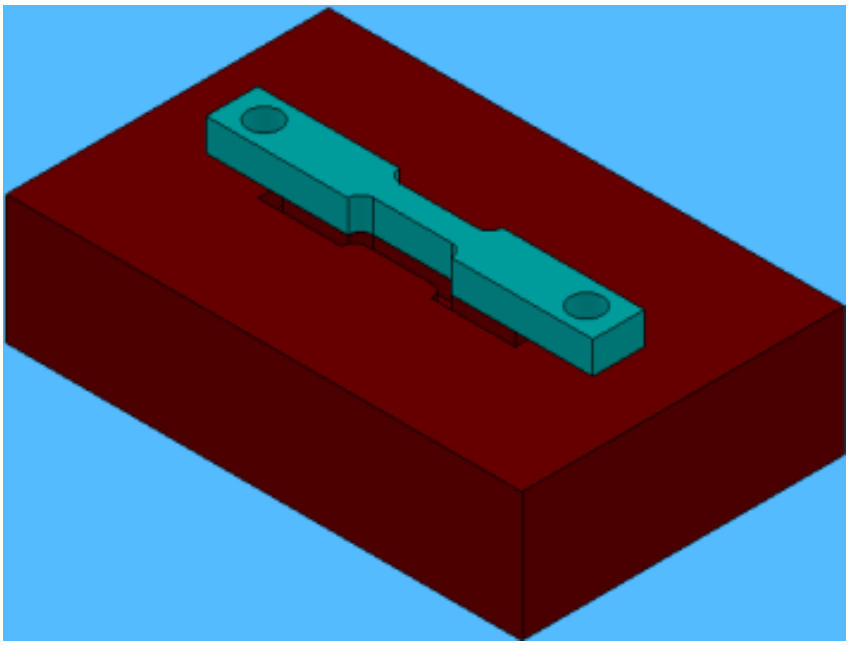

**Figure 13: Solidworks model of specimen cutting platform.**

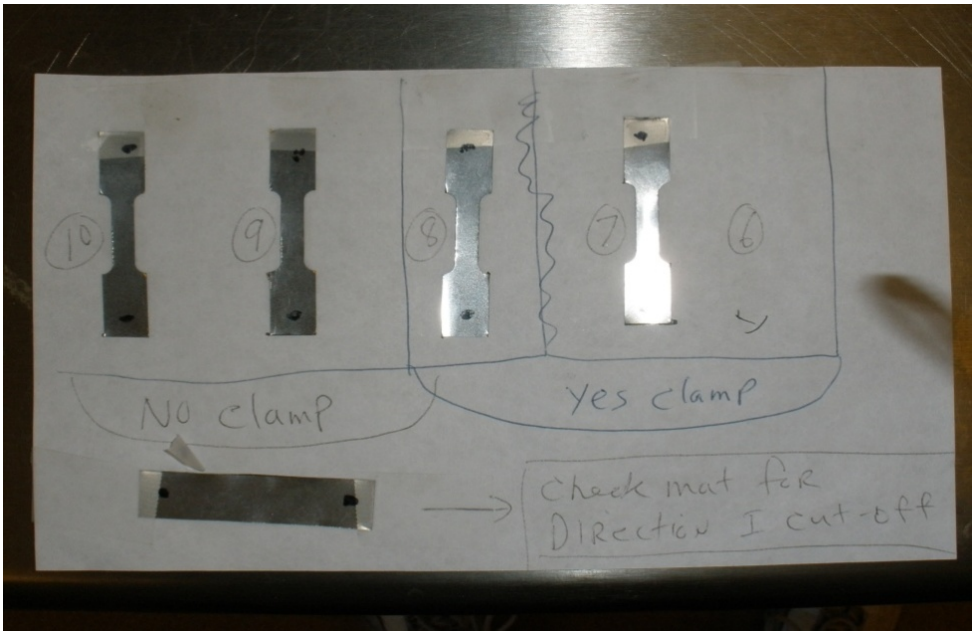


**Figure 14: "Dog bone" cut steel specimens.**

The steel were then cleaned using ethanol and acetone in order to remove any unnecessary oils from excessive touching. After cleaning, each of the steel specimens were numbered and ready for tensile and photogrammetry testing.

*PEDOT:PSS/PET:ITO Specimen Fabrication*

*PET:ITO Fabrication*

The PET:ITO layers were cut into a specific geometric "dog bone" shaped specimens like the steel specimens above. Using the specimen cutting platform designed by Todd Herman and James Howard of the Union College machine shop (Figure 13), the PET:ITO specimen were milled using a drill press in the Union College machine shop into precisely sized "dog bone" shaped specimens. The PET:ITO specimens were then cleaned using ethanol and acetone and then washed off with de-ionized water in order to remove any unnecessary oils from excessive touching. The PET:ITO The PET:ITO specimens were also numbered, but then PEDOT:PSS was applied to the ITO side of PET:ITO layer.

*PEDOT:PSS Layer Application Process*

After the PET:ITO fabrication process, each of the PET:ITO specimens were placed in a cleaned hexagon dish with the ITO side facing up. In order to determine the ITO side, a ohmmeter was used to read the resistance of each side of PET:ITO specimen. The side with no resistance reading (infinite) was PET while the side with a relatively small resistance was ITO. After placing the ITO face up in each dish, the 1:5 PEDOT:PSS solution was applied to each surface using one technique. The 1:5 PEDOT:PSS solution for PET:ITO specimen samples was applied using a pipette dropping technique. A pipette was used to collect 0.2 mL 1:5 PEDOT:PSS solution, and the solution was applied to the ITO surface one drop at a time. The drops started from the center of the ITO surface and then moving back and forth left and right while maintaining a homogenous solution across the cantilever part of the ITO (Figure 15).

**Figure 15: 1:5 PEDOT:PSS solution on PET:ITO "dog-shaped" specimen.**

*3.2 Macro-scale Testing*

Tensile testing of the steel and PEDOT:PSS/PET:ITO specimens was done using a tensile stage and a photogrammetry system. A stochastic pattern is deposited onto the surface of both types of specimens to clearly allocate the pixels in the camera facets. As the tensile stage puts the specimen under uni-axial tension, the photogrammetry system tracks points within the surface pattern to measure strain. The mechanical properties of these specimens were then calculated using the stress and strain data given by the tensile stage and photogrammetry techniques respectively.

*Steel Photogrammetry/Tensile Testing*

For photogrammetry/tensile stage measurements, the steel specimens were speckled with black and white paint in order to produce a stochastic pattern for the photogrammetry software to track strain. The speckle pattern for the steel samples was to add a coat of black paint for the background and then speckle on white paint for “dots” for the photogrammetry to track strain. The black and white paint was applied using a spray can at approximate distance of eighteen inches. This spraying distance was necessary in order to form smooth, homogenous speckle pattern. The best speckle pattern for steel was created by applying twenty passes of black paint (ten vertical and ten horizontal) and then two passes of white paint (one vertical and one

horizontal). After the first ten black passes, there was a minute pause to let the first layer of the black paint to dry. Afterwards, the steel samples were dried and then ready for testing (Figure 17).


**Figure 16: Stochastic pattern painting set-up**

**Figure 17: Speckled steel specimen.**

For this tensile stage set-up, a 100-lb. load cell was used along with MTESTQuattro materials testing system software. This tensile stage has the capability of being installed inside the SEM for more in-depth mechanical characterization of PEDOT:PSS. Just to recap, this tensile stage has the material specimen loaded into the center of the stage and is concordantly

pulled apart from each grip. This setup then applies a gradual load to the specimen past the yield point to failure while the grips hold the material in place (Figure 18).

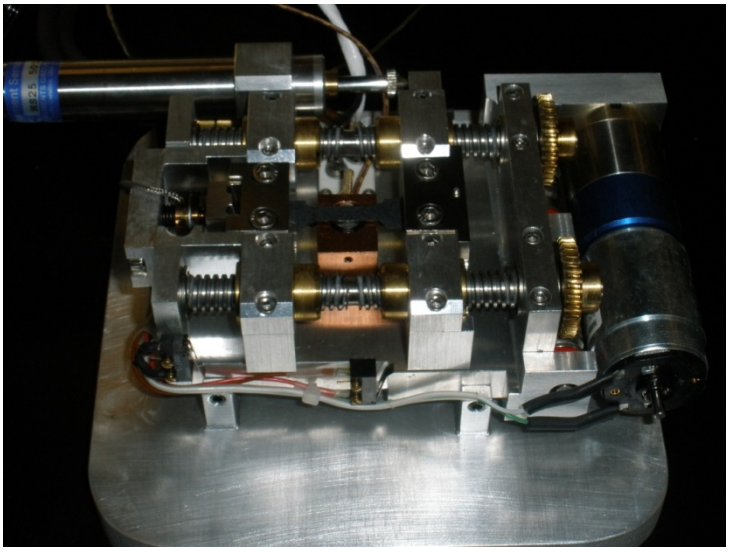

**Figure 18: Ernest F. Fullum tensile stage with 100 lb. load cell and fractured steel specimen.**

Due to the "dog bone" shape of the specimens, the maximum stress and strain occurring on the specimen is directly in the center of the specimen, where failure will occur. In order to record accurate mechanical properties, steel samples were tensile tested with the tensile stage in order to make sure the experimental values match universally known mechanical properties of steel.

For the photogrammetry set-up, a two-camera system was used along with ARAMIS v6 system software in the Union College composites lab (UCCL). Fiber-Lite, DC-950 Manfrotto lights were used to variably change the lighting of the specimens during photogrammetry measurements. The camera system was setup on an adjustable calibrated slider arm attached to an adjustable stage. The adjustable stage was hooked up to a tripod stand and an adjustable z-direction (depth) crank (Figure 19). The system was calibrated for the tensile stage setup.

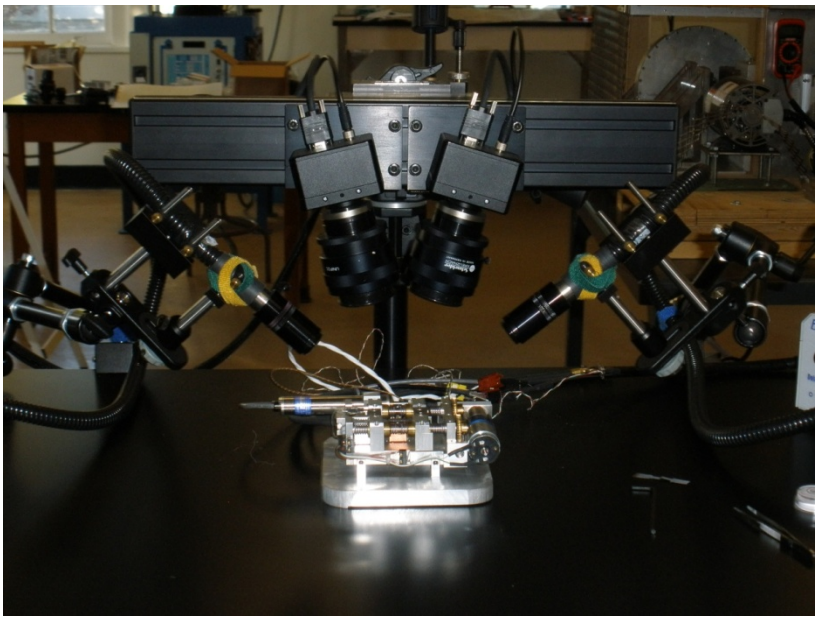

**Figure 19: ARAMIS M2 photogrammetry setup with tensile stage.**

For the photogrammetry calibration, the software and camera systems were calibrated using the ARAMIS v6 calibration process. With previous calibration notes, the lens, lens distance, ellipse quality, camera span, shutter time, and orientation were set at 50mm/15mm extensions, 235 mm, 0.8, 130 mm, 140 ms, and 90 degree role respectively. Using a specifically designed 12mm x 15mm cube, the photogrammetry system was calibrated by taking pictures of various cube orientations. After the calibration, the angle between the cameras, height variance, measured volume, and angle variance were found to be 28.7°, 10,485 µm, 20 mm/15 mm/5 mm, and -11.2/10.9° respectively. The temperature and relative humidity during this calibration were 23° C and 75% respectively. After the photogrammetry calibration, the tensile stage/photogrammetry set-up together was ready for tensile testing of steel specimens.

For accurate and precise measurements, the mechanical properties, like Young's modulus, of steel were measured with the tensile stage and then compared to known mechanical values of steel. The tensile stage was programmed to pull the steel specimens at a position rate of 0.1 inches per minute and a maximum load of 90 lbs. The tensile stage would gradually stretch

the specimens while increasing the load until failure. During the tensile stage testing, the photogrammetry system was used to capture position data of the specimen at certain load points. After failure, the load and position data was plotted and analyzed. From the tensile stage load data and photogrammetry positional data, the Young's Modulus of the steel specimen could be calculated. In order to calculate the stress, the difference of the two loads must be divided by the steel specimen cross-sectional area. The strain of the specimen was calculated by taking the difference between the two %Xstrain, tensile strain, points and dividing the difference by 0.01. The Young's Modulus of the specimen then was calculated by taking the stress divided by the strain. The experimental steel Young's Modulus values were then compared to actual accepted values of steel.

*PEDOT:PSS/PET:ITO Photogrammetry/Tensile Testing*

After testing and confirming accepted mechanical properties for the steel specimens, the photogrammetry/tensile stage was ready to test for mechanical properties of unknown materials, like PEDOT:PSS/PET:ITO specimen. For the photogrammetry stochastic pattern, the black paint background was applied on the PET side of the PEDOT:PSS/PET:ITO specimen. In other words, the black paint was applied to the side without the PEDOT:PSS. The black background was created by applying twenty passes (ten vertical and ten horizontal) of black paint using a spray can. After the first ten black passes, there was a minute pause to let the first layer of the black paint to dry. Once the black background was dried, the white paint speckle was created by applying two passes (one vertical and one horizontal) of white paint using a spray can. After these samples have dried, the PEDOT:PSS/PET:ITO samples were ready for testing (Figure 20).

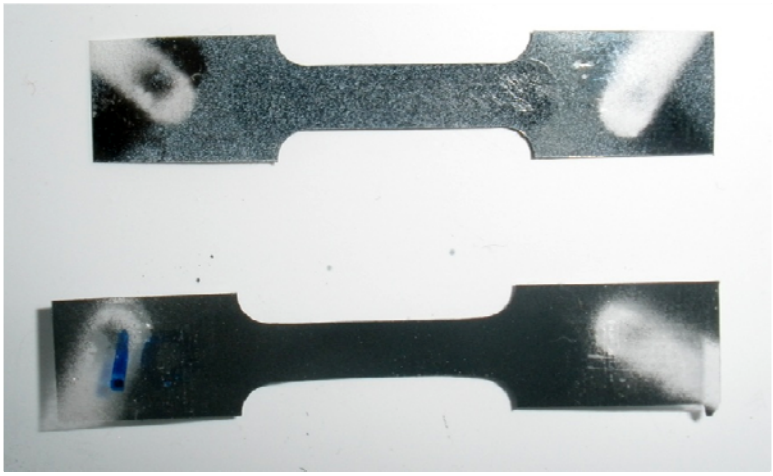

**Figure 20: Stochastic pattern of a PEDOT:PSS/PET:ITO specimen.**

The tensile stage was programmed to pull the steel specimens at a position rate of 0.5. inches per minute and a maximum load of 90 lbs. The tensile stage would gradually stretch the specimens while increasing the load until failure or plastic deformation. After failure or plastic deformation occurs, the tensile stage load data and photogrammetry positional data were used to calculate the Young's Modulus of the PEDOT:PSS specimens. The Young's Modulus was calculated by taking two load/position points during the testing. In order to calculate the stress, the difference of the two loads must be divided by the specimen cross-sectional area. The strain of the specimen was calculated by taking the difference between the two %Xstrain, tensile strain, points and dividing the difference by 0.01. The Young's Modulus of the specimen then was calculated by taking the stress divided by the strain. After tensile testing, scanning electron microscopy was used to characterize the PEDOT:PSS/PET:ITO specimens.

### *3.3 Microscale Analysis and SEM Characterization*

The scanning electron microscope (SEM) is an electron microscope that images the sample surface by scanning it with a high-energy beam of electrons. The SEM has an illumination filament source that sends high accelerating electron beam through a series of lenses

that focus the electrons onto a specific area or specimen and the backscattered electrons off the surface are collected by a detector and then imaged through SEM software. This technology allows for high magnified imaging and characterization of materials, like PEDOT:PSS. The nanoscaled imaging of the SEM will help identify any deformation, like crack propagation, undergoing on the PEDOT:PSS specimens under mechanical loading, like tension.

For this project, the Zeiss EVOO50 SEM in Olin Laboratory at Union College was used to characterize the PEDOT:PSS/PET:ITO specimens (Figure 21). An EHT voltage of 5 kV and an I probe current of 220 pA were the settings used to examine the specimens. A wobble technique was used to increase magnification and focus of the specimens in order to understand the micro-scale structure before and after tensile testing.


**Figure 21: Zeiss EVOO50 SEM setup.**

The untested and tested PEDOT:PSS/PET:ITO specimens were analyzed under the SEM in order to investigate any deformation, such as crack propagation, that may have occurred during tensile testing. The PEDOT:PSS/PET:ITO specimens were analyzed before and after tensile testing at same three regions of interest in order to compare before and after deformation

of the PEDOT:PSS. The deformation characterization of these specimens were analyzed and used to figure out the maximum tensile application these specimens could undergo before deformation and decrease solar device efficiency.

# 4. Discussion of Results

One of the goals of this project was to determine the mechanical properties, such as Young's Modulus, of PEDOT:PSS/PET:ITO. A second objective was to examine the deformation formation of PEDOT:PSS and characterize the deformation under tensile applications. Lastly, the question of interfacial interactions between PEDOT:PSS and PET:ITO, and how it affects the overall strength of the device were investigated. In this section, the results of the subsequent tests discussed in the previous section will be presented.

## *4.1 Steel Tensile Testing Results*

The first step towards these goals was complete characterization of PEDOT:PSS and PET:ITO. Once this was completed, a comprehensive literature review determined any relevant tensile test results and analysis of PEDOT:PSS. After finding published mechanical properties of PEDOT:PSS and PET:ITO, the tensile stage and photogrammetry system needed to be calibrated and initially tested with a known material, steel. The purpose of using a different material was to refine the experimental technique before using the materials in question. The steel tensile testing experimental data explained in the procedure is shown in Table 3.

**Table 3: Steel Tensile Testing Results for Steel Specimens 1, 2, and 3; Testing was stopped at 40, 42, and 39 lb. force respectively.**

| Steel Specimen #1 | | Steel Specimen #2 | | Steel Specimen #3 | |
|---|---|---|---|---|---|
| **Force (lb)** | **Avg. %εx** | **Force (lb)** | **Avg. %εx** | **Force (lb)** | **Avg. %εx** |
| 0 | 0 | 0 | 0 | 0 | 0 |
| 7.33 | 0.096 | 8.06 | 0.0995 | 6.23 | 0.0869 |
| 39.32 | 0.5336 | 41.24 | 0.5613 | 15.55 | 0.1923 |
| - | - | - | - | 27.69 | 0.3368 |
| - | - | - | - | 39.28 | 0.7585 |

Once the experimental data has been gathered, it is necessary to determine the Young's Modulus of the specimen. The Young's Modulus is the stress divided by the strain of the specimen. The stress of the specimen can be modeled by Equation 3

$$\sigma = \frac{\Delta F}{A} \qquad \text{Equation 3}$$

where $\Delta F$ is the intermediate force values gathered by the load cell and $A$ is the cross-sectional area of a steel and PEDOT:PSS/PEET:ITO specimen which was determined to be 0.000275in$^2$ and 0.000975 in$^2$ respectively. Once the stress was determined, the strain of the specimen can be modeled by Equation 4.

$$\varepsilon = \frac{\Delta\%\boldsymbol{\varepsilon x}}{0.01} \qquad \text{Equation 4}$$

where $\Delta\%\boldsymbol{\varepsilon x}$ is the intermediate percent tensile strain values gathered by the photogrammetry system and the 0.01 is a conversion from percent to inches/inches. With the stress and strain, the Young's Modulus could be calculated by Equation 5

$$E = \frac{\sigma}{\varepsilon} \qquad \text{Equation 5}$$

where σ is the stress calculated in Equation 3, and Δε is the change in strain gathered from the same intermediate forces chosen in Equation 4. Table 4 shows the experimental Young's Modulus values of the three steel specimens.

**Tables 4: Steel Tensile Testing Young's Moduli.**

| Steel Specimen #1 | Steel Specimen #2 | Steel Specimen #3 |
|---|---|---|
| Young's Modulus ($10^{-6}$ psi) | Young's Modulus ($10^{-6}$ psi) | Young's Modulus ($10^{-6}$ psi) |
| 22.2 | 26.2 | 26.3 |

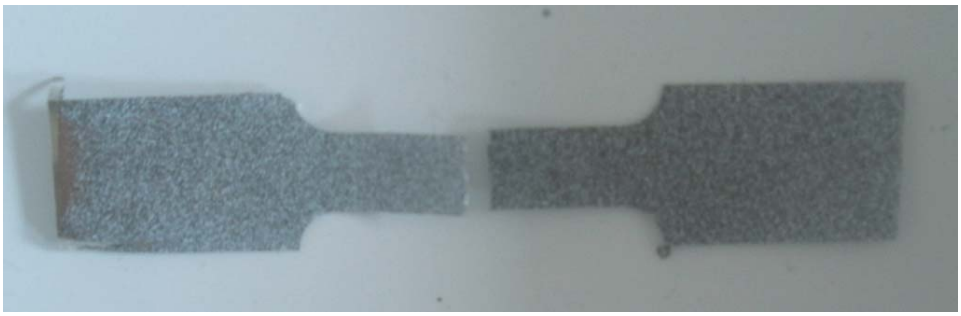

**Figure 22: Steel tensile tested specimen.**

The accepted Young's Modulus value for steel is around 29 million psi. The experimental error of the steel specimens' #1, #2, and #3 were -23.4, -9.7, and -9.3 percent respectively. Due to the relatively close experimental values to accepted values of steel, the tensile testing system was working properly and ready for PEDOT:PSS testing.

*4.2 PEDOT:PSS/PET:ITO Tensile Testing Results*

The PEDOT:PSS/PET:ITO specimens were tensile tested exactly the same as the steel specimens. The PEDOT:PSS/PET:ITO experimental data is shown in Table 5.

**Table 5: PEDOT:PSS Tensile Testing Result for PEDOT:PSS, Testing was stopped at 14 lb. force.**

| **PEDOT:PSS Specimen #1** | | **PEDOT:PSS Specimen #2** | |
|---|---|---|---|
| **Force (lb)** | **Avg. %εx** | **Force (lb)** | **Avg. %εx** |
| 0 | 0 | 0 | 0 |
| 7.95 | 3.210 | 0.5 | 1.120 |
| 13.75 | 4.154 | 6.4 | 2.834 |

Once the experimental data has been gathered, it is necessary to determine the Young's Modulus of the specimen. The Young's Modulus of PEDOT:PSS/PET:ITO was calculated using Equations 3,4, and 5 shown previously in the section. Table 6 shows the experimental Young's Modulus values of the PEDOT:PSS/PET:ITO specimen.

**Table 6: PEDOT:PSS Tensile Testing Young's Moduli.**

| PEDOT:PSS Specimen #1 | PEDOT:PSS Specimen #2 |
|---|---|
| Young's Modulus (ksi) | Young's Modulus (ksi) |
| 452 | 392 |

**Figure 23: PEDOT:PSS/PET:ITO tensile tested specimen.**

The few articles that presented mechanical properties of PEDOT:PSS and PET:ITO published Young's Moduli for each material of around 261 ksi and 400-600 ksi respectively. The PEDOT:PSS/PET:ITO specimens had an average Young's Modulus value of around 422 ksi, which is in between the two published Young's Modulus values of PEDOT:PSS and PET:ITO. After tensile testing, the characterization of PEDOT:PSS/PET:ITO specimens in the SEM was conducted in order to investigate the deformation of the specimen.

*4.3 PEDOT:PSS/PET:ITO Microscale Analysis and SEM Results*

The PEDOT:PSS/PET:ITO specimens, unspeckled and untested, were first analyzed using scanning electron microscopy (SEM). The SEM revealed the PEDOT:PSS layer of the specimens to have a heterogeneous make-up. The PEDOT:PSS layer was composed of dendritic-like structures throughout the whole specimen (Figure 24). Phase separation of the layer was the

cause of the PEDOT:PSS crystallization. The phase separation may have been caused by a lack of rinsing off the PET:ITO specimen with de-ionized water before applying PEDOT:PSS. The acetone left on the ITO surface during the PEDOT:PSS application would have interacted with the PEDOT:PSS and changed the overall appearance of the layer.

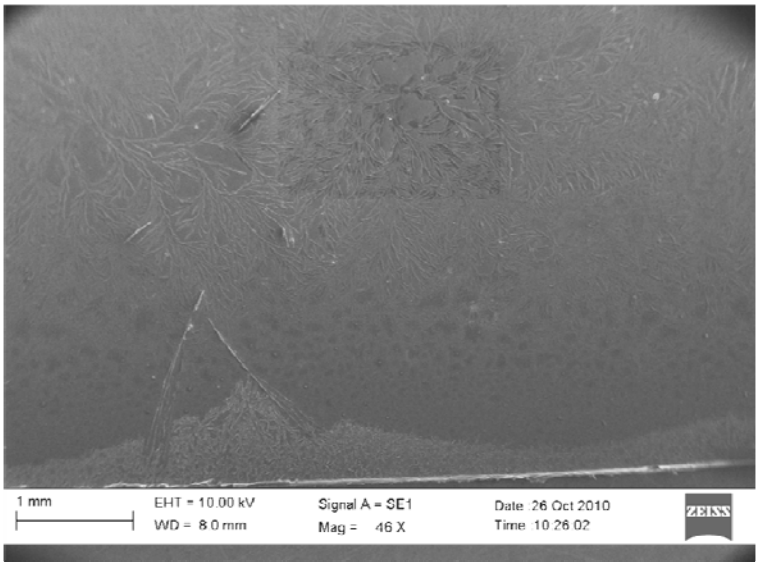


**Figure 24: Crystalline microstructure of PEDOT:PSS/PET:ITO.**

The SEM also revealed further evidence of PEDOT:PSS layer not having a uniform surface. The untested and unspeckled PEDOT:PSS/PET:ITO specimens also showed a pitted microstructure (Figure 25). The PEDOT:PSS layer at higher magnifications had some spots of microstructure pitting due to solvent evaporation. Solvent evaporation was caused by the specimen being exposed to ambient air and drying too quickly during fabrication. This pitted microstructure could limit the layer to layer interaction with the other layers and decrease the overall efficiency of the solar device.

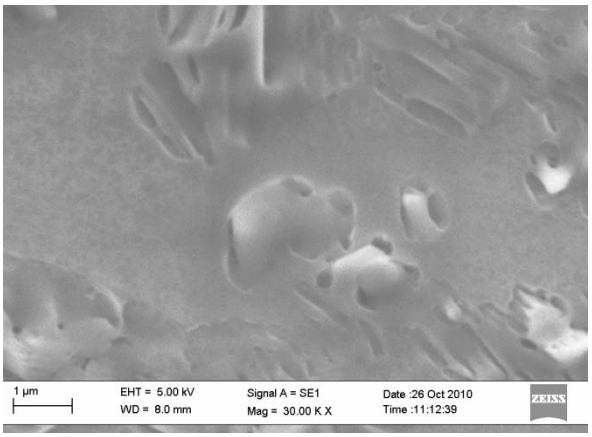


**Figure 25: Pitted microstructure of PEDOT:PSS/PET:ITO.**

After analyzing an untested and unspeckled specimen, a speckled, untested PEDOT:PSS/PET:ITO specimen was then analyzed under the SEM (Figure 26). The section viewed of this specimen does not appear to have the heterogeneity or dendritic-like structures present in the microstructure of PEDOT:PSS like the previous images. Besides the microstructure, the paint particles from the stochastic pattern also appeared to have interacted with the PEDOT domains of the specimen, as shown by the big mounds underneath the paint particles. This interaction may have been caused by the enamel paint solvent. This reaction may have significantly changed the structure and mechanical properties of PEDOT:PSS.

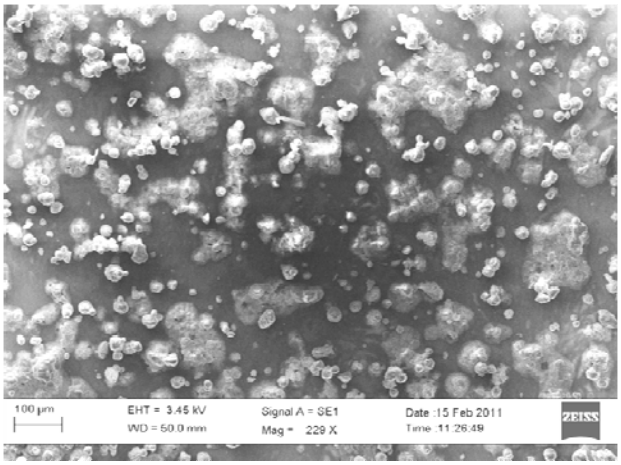


**Figure 26: SEM imaging of PEDOT:PSS with stochastic pattern before tensile testing.**

The PEDOT:PSS/PET:ITO specimens were then analyzed under the SEM after tensile testing. The specimens had significant gapping and crack propagation (Figure 27). The SEM image reveals rigid structure particles all over the specimen. These rigid segments may have been result of the dendritic-like structure of PEDOT:PSS stretching and breaking into smaller segments. The untested and tested specimen images exhibit different microstructures, which may explain the complete difference in the characterization of these images. Even though the different microstructures were interesting, the important feature of these specimens was the uniform crack propagation along the PEDOT:PSS layer.

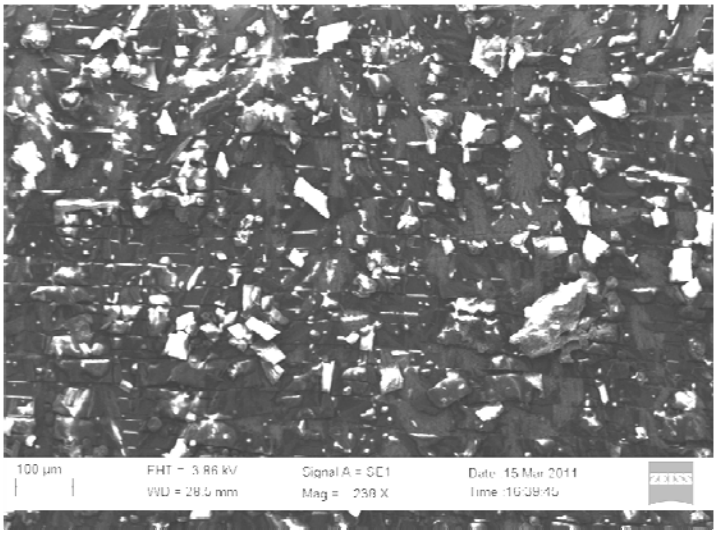


**Figure 27: SEM imaging of PEDOT:PSS with stochastic pattern after tensile testing.**

SEM analysis of tested PEDOT:PSS/PET:ITO specimens showed a more clear look at the crack propagation of PEDOT:PSS (Figures 28, 29, and 30). The specimen in these images is being pulled with a uni-axial load in the up and down directions of the paper. The width and length of the specimens had decreased and increased after testing due to Poisson's ratio. The crack propagation along the PEDOT:PSS layer appears throughout the specimen, while occurring more often in the middle of the specimen than the ends. This increase crack

propagation in the middle of the specimen is from higher stress concentrations occurring at the middle of the specimen. The crack widths were approximately around 10 microns.

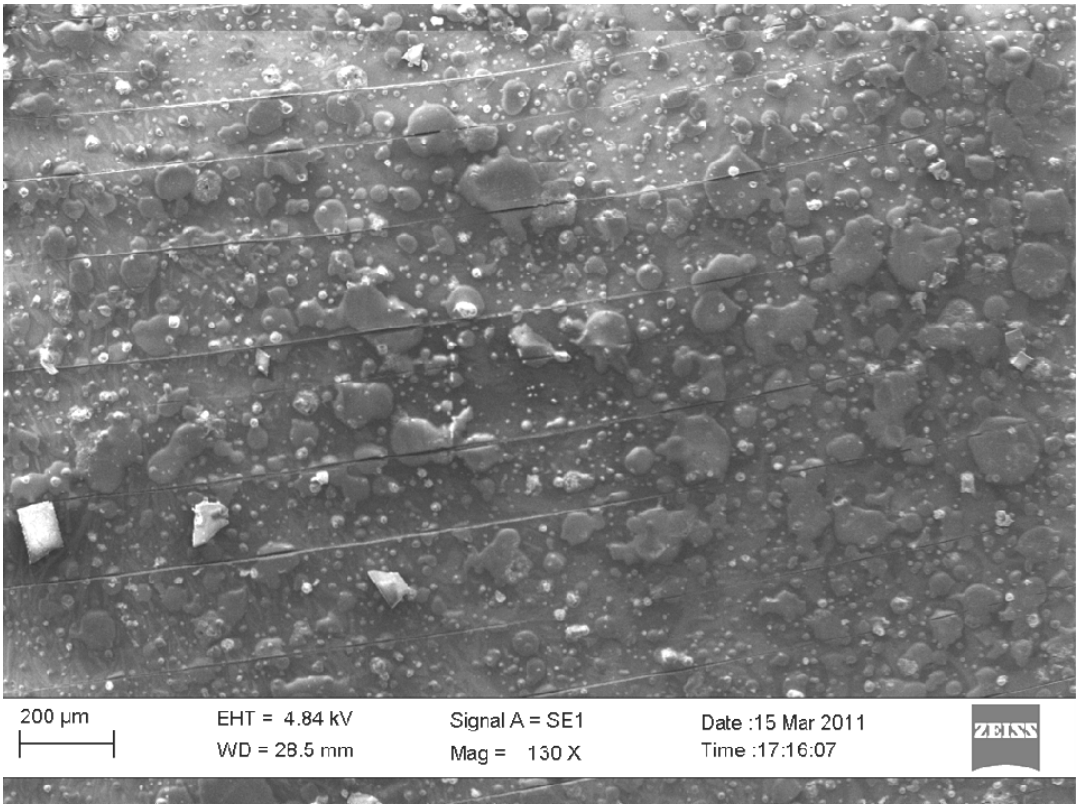


**Figure 28: SEM imaging of PEDOT:PSS with crack propagation after tensile testing.**

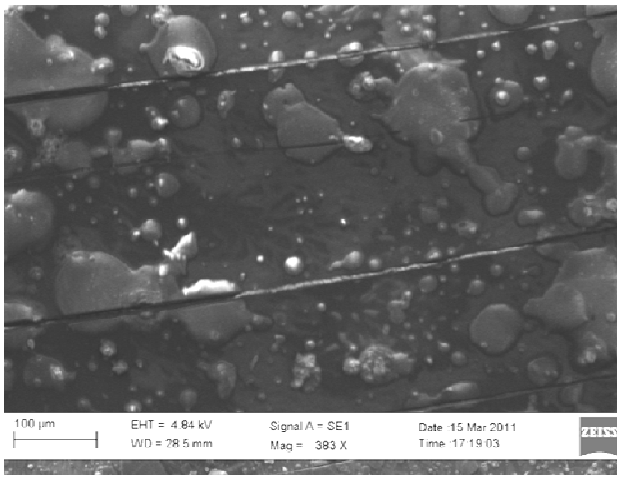


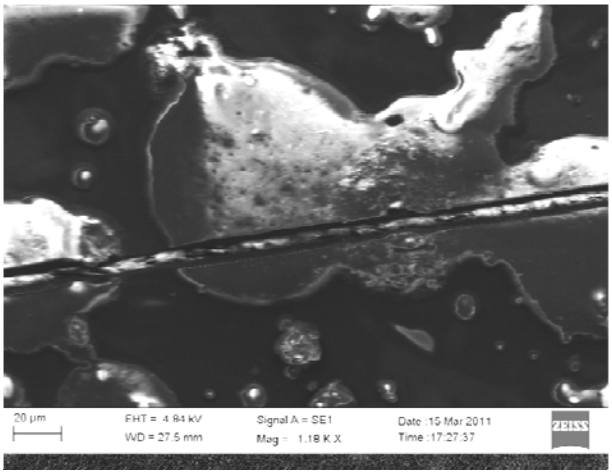


**Figures 29 and 30: Highly magnified SEM imaging of PEDOT:PSS with crack propagation after tensile testing.**

The edges of the tested PEDOT:PSS/PET:ITO specimens were then analyzed with the SEM (Figure 31). The edge of the specimens exposed the PEDOT:PSS/PET:ITO layers start to separate and form  mica-like structure of separate layers. This empirical evidence may show de-lamination of the specimen during tensile testing. This phenomenon would significantly decrease the mechanical strength and layer to layer interaction of the solar cell. Overall, the efficiency of the solar device would decrease significantly.

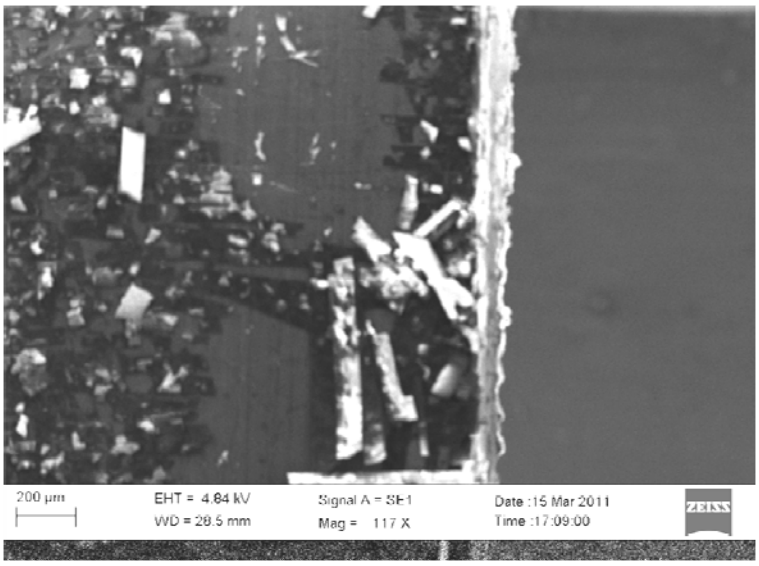


**Figure 31: SEM imaging of edging of PEDOT:PSS and PET:ITO after tensile testing.**

Further SEM analysis was done on the cross-section of the PEDOT:PSS/PET:ITO specimen after failure (Figure 32). The cross-sectional image revealed significant deformation of the whole specimen. The height and width of the PEDOT:PSS/PET:ITO specimen after failure was approximated at 90 microns ± 20 microns and 0.1 mm ± 0.01 mm respectively. The original height and width of just the PET:ITO layer was around 200 microns and 5.1 mm respectively. The cross-sectional area of the specimen decreased to around 25% of the original cross-sectional area size.  Overall, the cross-sectional area of the specimen decreased significantly due to Poisson's ratio during tensile testing.

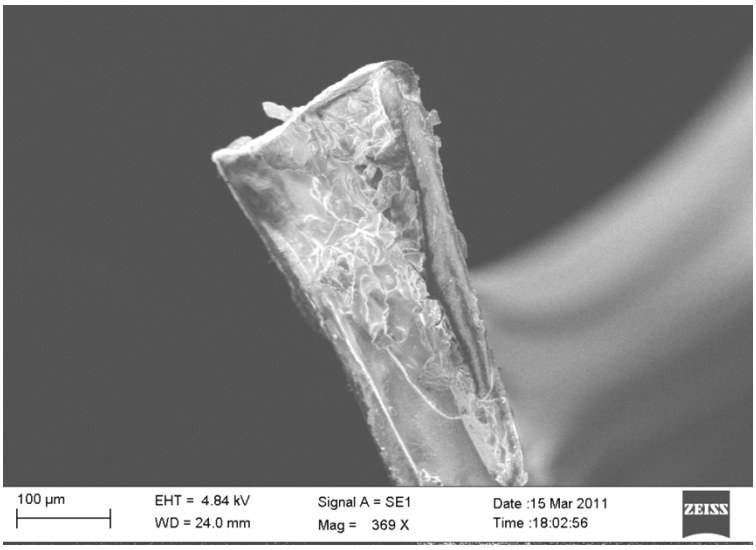


**Figure 32: SEM imaging of cross-section of PEDOT:PSS and PET:ITO after tensile testing failure.**

Just to recap, the tensile testing and characterization of PEDOT:PSS/PET:ITO specimens revealed significant flaws that will decrease the overall efficiency of the solar cell. The fabrication process of PEDOT:PSS/PET:ITO caused significant heterogeneity and solvent evaporation of PEDOT:PSS which will affect the layer to layer interactions of the solar cell. The tensile testing caused the PEDOT:PSS/PET:ITO specimens to have PEDOT:PSS crack propagation and possible specimen de-lamination which will decrease the conducting properties of PEDOT:PSS and the efficiency of the solar cell. In order to improve the solar cell's efficiency, the PEDOT:PSS/PET:ITO specimen flaws must be addressed and solved in future work.

# 5. Conclusion and Recommendations

The goal of this project was to investigate the mechanical strength and characterization of PEDOT:PSS. In past years, solar research has been focused on improving solar devices by changing the method of fabrication. This project investigates the mechanical properties of solar nanocomposite layers of a solar device in order to find a correlation between mechanical properties of each material and the overall efficiency of the solar cell. The interface between nanocomposite material layers, such as PEDOT:PSS and PET:ITO, is usually an area for points of failure. The further investigation of failure points at each interface of the solar device will lead to a better understanding of the solar device and its efficiency. Furthermore, once these points are determined, the fabrication technique can be changed for improvement.

Progress has been made with regards to determining the mechanical properties and characterization of PEDOT:PSS under tensile applications. During tensile testing, the PEDOT:PSS/PET:ITO specimens had an average Young's Modulus value of 422 ksi, which is in the range of accepted PET Young's Modulus values. suggests that the mechanical properties of the specimen are dictated by PET:ITO. After tensile testing, the PEDOT:PSS on the specimen showed deformation under naked eye observation. The SEM characterization of tested PEDOT:PSS/PET:ITO revealed crack propagation of PEDOT:PSS along the specimen. Crack formation in the PEDOT:PSS layer would interfere with hole conducting process of the material in the solar device. The SEM characterization of untested PEDOT:PSS/PET:ITO specimens revealed significant solvent evaporation (pitted microstructure), heterogeneity (crystalline microstructure), and solution etching of the PEDOT:PSS layer. Overall, the crack propagation and various microstructure flaws will significantly decrease the overall solar cell efficiency.

In order to find ways to improve the solar cell efficiency, there are some recommendations for future work with tensile testing, SEM characterization, fabrication, and photogrammetry. The current tensile testing results only prove crack propagation of PEDOT:PSS at relatively high loads, not at intermediate or low loads. Tensile testing PEDOT:PSS/PET:ITO specimens under the SEM would allow for the user to mechanically characterize when crack propagation begins. This knowledge will help determine at what loads the PEDOT:PSS layer begins to fail and the different applications the solar cell can withstand without affecting its efficiency. It is highly recommended for future tensile testing under the SEM.

For future fabrication work, it is recommended to emphasize the importance of rinsing off the PET:ITO substrate with de-ionized water before applying PEDOT:PSS. This action will eliminate the possibility of crystallization of PEDOT in the PEDOT:PSS layer and allow for a more homogeneous solution. A more homogeneous solution will allow for better hole conducting properties and hopefully more layer to layer interaction. In order to improve the layer to layer interactions of the solar cell, uniform layers are also necessary in making sure the solar cell will have maximum conducting properties. The pipette drop technique of PEDOT:PSS left a relatively curved top surface, which could decrease the layer to layer interaction and solar cell efficiency. It is also recommended to look into a spray-coating technique for the fabrication process of PEDOT:PSS. Spray-coating would be an easy way to apply a thin, uniform layer of material onto the solar device, which would ensure higher interface interaction and device efficiency.

For photogrammetry recommendations, the stochastic paint pattern on the PEDOT:PSS layer may have caused significant changes in the microstructure. The SEM characterization found significant interaction with the paint particles and the PEDOT:PSS layer. The paint solvent

may have bonded with free PEDOT domains, and this chemical interaction may cause the paint solvent to etch or eat away at the PEDOT:PSS layer. This process may cause a significant decrease PEDOT domain interaction and layer to layer interaction of the solar device. It is recommended to continue experimenting with different types of paint on top of the PEDOT:PSS layer and analyzing the morphology of the PEDOT:PSS.

Besides investigating PEDOT:PSS, it is necessary to continue investigating mechanical properties of the other solar nanocomposite layers of the solar device. Each layer will affect the overall mechanical properties of the solar device, and the layer to layer interactions between nanocomposite layers should be characterized. In order to improve the efficiency of the solar device, the characterization and morphology of the whole solar device will help show where the solar device needs improvement, specifically with materials or fabrication.

# 6. References


1. Randolph, John, and Gilbert M. Masters. *Energy for Sustainability: Technology, Planning, Policy*. Washington, D.C.: Island, 2008. Print.
2. Montgomery, Scott L. *The Powers That Be: Global Energy for the Twenty-first Century and beyond*. Chicago: University of Chicago, 2010. Print.
3. McElroy, Michael B. *Energy: Perspectives, Problems, and Prospects*. Oxford: Oxford UP, 2010. Print.
4. Bryce, Robert. *Power Hungry: the Myths of "green" Energy and the Real Fuels of the Future*. New York, NY: PublicAffairs, 2010. Print.
5. Shahan, Zachary. "Wind Turbines Based on Jet Engines 3-4 Times More Efficient & Coming to Market? [VIDEO] – CleanTechnica." *CleanTechnica*. 26 Jan. 2010. Web. 01 Oct. 2010. <http://cleantechnica.com/2010/01/26/wind-turbines-based-on-jet-engines-3-4-times-more-efficient-coming-to-market-video/>.
6. *Photovoltai cs: Design and Installation Manual : Renewable Energy Education for a Sustainable Future*. Gabriola Island, B.C.: New Society, 2004. Print.
7. Kehlbeck, Joanne D., Michael E. Hagerman, Brian D. Cohen, Jennifer Eliseo, Melissa Fox, William Hoek, David Karlin, Evan Leibner, Emily Nagle, Michael Nolan, Ian Schaefer, Alexandra Toney, Michael Topka, Richard Uluski, and Charles Wood. "Directed Self-Assembly in Laponite/CdSe/Polyaniline Nanocomposites." *Langmuir* 24 (2008): 9727-738.
8. Tolliver, Todd. "Solar Manufacturing Strategies." Solar Technology. New York, Schenectady. Winter 2008. Lecture.
9. Michael R. Topka “Nanomorphology Studies of Poly(3,4-Ethylene-Dioxythiophene) in Organic-Inorganic Photovoltaic Devices.” Thesis. Union College, 2009. Print.

10. Khang, Dahl-Young, Jianliang Xiao, Coskun Kocabas, Scott Maclaren, Tony Banks, Hanqing Jiang, Yonggang Y. Huang, and John A. Rogers. "Molecular Scale Buckling Mechanics in Individual Aligned Single-Wall Carbon Nanotubes on Elastomeric Substrates." *Nano Letters* 8.1 (2008): 124-30.
11. *Basic Research Needs For Solar Energy Utilization*. Rep. Argonne National Laboratory, 21 Apr. 2005. Web. 20 Nov. 2009.
12. Hwang, Euiyong, K.M. De Silva, Chad B. Seevers, Jie-Ren Li, Jayne C. Garno, and Evgueni E. Nesterov. "Self-Assembled Monolayer Initiated Electropolymerization: A Route to Thin-Film Materials with Enhanced Photovoltaic Performance." *Langmuir* 24 (2008): 9700-706.
13. Yunus, Sami, Anne Attout, and Patrick Bertrand. "Controlled Aniline Polymerization Strategies for Polyaniline Micro and Nano Self-Assembling into Practical Electronic Devices." *Langmuir* 25 (2009): 1851-854.
14. Rao, YuanQiao, and John M. Pochan. "Mechanics of Polymer - Clay Nanocomposites." *Macromolecules* 40 (2007): 290-96.
15. *SCP | Rockwood Additives*. Web. Fall 2009.
16. Whitesides, G.; Grzybowski, B. *Science* 2002, 295, 2418-2421.
17. Suo, Z. *et al.*, "Mechanics of rollable and foldable film-on-foil electronics", *Applied Physics Letters,* Vol. 74, No. 8 (1999) pp. 1177-1179.
18. Lang, Udo, and Jurg Dual. "Mechanical Properties of Baytron P." *IEEE Xplore* (2004): 230-36. Web. 26 Jan. 2010. <http://http://www.ieeexplore.ieee.org/Xplore/guesthome.jsp>.
19. Roark, Raymond J., and Warren C. Young. *Roark's Formulas for Stress and Strain.* New York: McGraw-Hill, 1989. Print.

20. H. Okuzaki, H. Suzuki, T. Ito, Electrically driven PEDOT/PSS actuators, Synthetic Metals, Volume 159, Issues 21-22, International Conference on Science and Technology of Synthetic Metals, Porto de Galinhas Pernambuco, Brazil, July 6-11, 2008 - ICSM 2008, November 2009, Pages 2233-2236, ISSN 0379-6779, DOI: 10.1016/j.synthmet.2009.07.054.
21. M. M. de Kok, M. Buechel1, S. I. E. Vulto, P. van de Weijer, E. A. Meulenkamp, S. H. P. M. de Winter, A. J. G. Mank, H. J. M. Vorstenbosch, C. H. L. Weijtens, V. van Elsbergen, *Phys. Stat. Sol. (A)* **2004**, *201*, 1342.

22. Zhou, Jin X. "Characterization of Drop-on-demand Microdroplet Printing." *The International Journal of Advanced Manufacturing Technology* 48.1-4 (2009): 243-50. Print.
23. Deffeyes, Kenneth S. *Hubbert's Peak: the Impending World Oil Shortage*. Princeton, NJ: Princeton UP, 2008. Print.

# 7. Appendices

Appendix A: PEDOT:PSS and PET:ITO Application Procedure

Materials:

PET:ITO
Ethanol
Acetone
De-ionized Water
PEDOT:PSS
Paper Trays
Chem Wipes
Paper
Glassware (Beaker, pipets)
EPP
Gloves
Q-tips
Ohmmeter
Calibrated Centrifuge Tubes

ITO Cleaning Process:

1st Stage of Cleaning

(1) Wash hands and wear gloves
(2) 50/50 solution of Ethanol and Deionized water in a beaker
(3) Place cut "dog bone" shape ITO specimens in beaker
(4) Leave in hood with cover for 1-2 days

2nd Stage of Cleaning

(1) Wash hands and wear gloves
(2) Pour most of 50/50 solution of Ethanol and Deionized water in an empty beaker (Put in hood)
(3) Remove "dog-bone" ITO specimens out of the remaining solution in the original beaker
(4) Place specimens on clean field (piece of paper with chem. Wipes)
(5) Let specimens dry for 30 minutes in ambient air
(6) Apply acetone onto ITO with Q-tip and wipe off any unnecessary oil/marks
(7) Rinse specimen with de-ionized water to remove acetone
(8) Let specimen dry for 30 minutes in ambient air
(9) Place specimen in a paper tray and cover

ITO Side Check Process:

(1) With a dry specimen, check the sides of the specimen with a ohmmeter
(2) A small resistance reading indicates ITO side
(3) A large (infinite) resistance is the PET side

PEDOT:PSS Solution Mixing Process:

(1) Wash hands and wear gloves
(2) Shake PEDOT:PSS bottle in order to get a homogeneous solution
(3) With a glass pipet, mix in a calibrated centrifuge tube 1 part PEDOT:PSS : 6 parts Deion. water
(4) Do NOT reuse pipet (Throw away through chemistry department)

PEDOT:PSS Application Process:

(1) Wash hands and wear gloves
(2) With 1:5 PEDOT:PSS/Water solution, put 0.2 - 0.25 mL of solution in EPP with clean glass pipet
(3) With another clean pipet, start applying solution evenly onto ITO specimen in paper tray
(4) NOTE: Apply PEDOT:PSS solution slowly and remember the amount of solution placed
(5) Place top tray on specimen, and place it in ambient air to let dry for 1-3 days

Appendix B: SEM Procedure


(1) Turn on system (Green Button)
(2) Login
(3) Make sure nothing is set on the stage
(4) Initialize the stage or set the x,y, and angle stage components to 50 mm, 50 mm, and 315 respectively (center the stage)
(5) Turn on beam gun to see if SEM camera is centered on the "donut."
(6) If not, adjust the gun align specifically emission and adjust until picture of donut is clear.
(7) After, turn off beam gun and vent out the system (in order to put in sample).
(8) Tape dog bone specimen onto "clip" platform with copper tape.
(9) Once vented, open SEM and place the platform with specimen onto stage (make sure the flat edge of the platform fits against the adjoined flat edge of the stage).
(10) Close SEM and vent on (pump) the system, then turn on beam gun.
(11) After, adjust beam settings: kV <= 5 kV (better quality images with PEDOT:PSS)
(12) Open up Data zone settings (so magnification is included in parameters)
(13) Use focus and magnification knobs in order to increase image quality and adjust specimen region of interest

*In order to improve focus, try using stimulater x and y knobs in order to see if focus increases (ask Mr. Hooker or Professor Cortez to help)

**Also, use wobble technique (cannot use focus with this technique)

- In order to do this, turn wobble on and adjust x and y knobs in order to limit shifting wobble in image in either x or y directions (more image clearness)

(14) In order to take photos, click on photo button on top of the screen on the main menu.
(15) Also, adjust brightness and contrast of image in order to get higher image clarity.

(16) After photo, click “unfreeze” and change frame average in order to return to SEM imaging
(17) After SEM imaging, to turn off the system turn off beam and vent out in order to remove the platform and specimen.
(18) In order to take specimen out of the SEM, vent the SEM and open the SEM and place the platform with specimen onto stage
(19) After taking out the specimen, close the SEM and vent on (pump) the SEM (keep it on vacuum settings), log off software, turn off computer, and press the stand by button (yellow button).